

Dynamics of Large-Scale Solar-Wind Streams Obtained by the Double Superposed Epoch Analysis: 3. Deflection of the Velocity Vector

Y.I. Yermolaev¹ · I.G. Lodkina¹ · M.Y. Yermolaev¹

Received: 24 February 2018 / Accepted: 28 May 2018 / Published online: 19 June 2018
© Springer Nature B.V. 2018

Abstract This work is a continuation of our previous articles (Yermolaev *et al.* in *J. Geophys. Res.* **120**, 7094, 2015 and Yermolaev *et al.* in *Solar Phys.* **292**, 193, 2017), which describe the average temporal profiles of interplanetary plasma and field parameters in large-scale solar-wind (SW) streams: corotating interaction regions (CIRs), interplanetary coronal mass ejections (ICMEs), including both magnetic clouds (MCs) and ejecta), and sheaths as well as interplanetary shocks (ISs). Changes in the longitude angle, φ , in CIRs from -2° to 2° agree with earlier results (*e.g.* Gosling and Pizzo, 1999). We have also analyzed the average temporal profiles of the bulk velocity angles in sheaths and ICMEs. We have found that the angle φ in ICMEs changes from 2° to -2° , while in sheaths it changes from -2° to 2° (similar to the change in CIRs), *i.e.* the angle in CIRs and sheaths deflects in the opposite sense to ICMEs. When averaging the latitude angle ϑ on all the intervals of the chosen SW types, the angle ϑ is almost constant at $\sim 1^\circ$. We made for the first time a selection of SW events with increasing and decreasing ϑ and found that the average ϑ temporal profiles in the selected events have the same “integral-like” shape as for φ . The difference in φ and ϑ average profiles is explained by the fact that most events have increasing profiles for the angle in the ecliptic plane as a result of solar rotation, while for the angle in the meridional plane, the numbers of events with increasing and decreasing profiles are equal.

Keywords Velocity vector · Solar wind streams · ICME · Sheath · CIR

1. Introduction

The quiet and uniform solar wind (SW) at 1 AU extends radially. Non-stationarity and heterogeneity in the solar atmosphere lead to the formation of disturbed solar wind structures, which have different speeds and interact with the surrounding quasi-stationary SW streams and with each other. One experimental evidence of stream interactions is the SW deflection

✉ Y.I. Yermolaev
yermol@iki.rssi.ru

¹ Space Research Institute (IKI), Russian Academy of Sciences, Profsoyuznaya 84/32, Moscow 117997, Russia

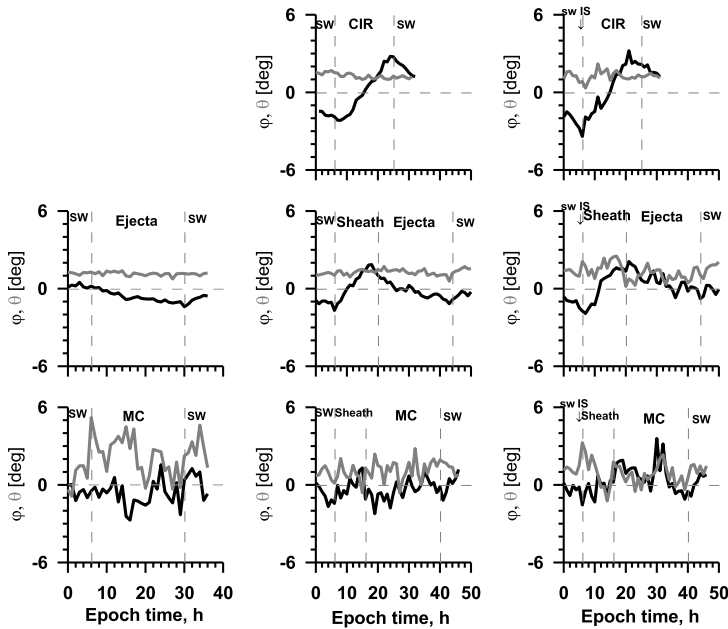


Figure 1 Time variation in longitude φ (black line) and latitude ϑ (gray) bulk velocity angles obtained by the double superposed epoch analysis in eight sequences of SW events: (1) SW/CIR/SW, (2) SW/IS/CIR/SW, (3) SW/ejecta/SW, (4) SW/sheath/ejecta/SW, (5) SW/IS/sheath/ejecta/SW, (6) SW/MC/SW, (7) SW/sheath/MC/SW, and (8) SW/IS/sheath/MC/SW. The dashed vertical lines show the boundaries of the SW types that are indicated in the upper parts of each panel.

relative to the radial direction. Although the velocity vector measured in separate events can vary along an individual path, when averaging on a large number of events of identical SW type, the change in the stream direction shows a steady trend. For example, corotating interaction regions (CIRs) are a consequence of the spatial variability in the coronal expansion and solar rotation that cause the interaction of fast streams from coronal holes with slow streams from coronal streamer belts. This interaction results in compression of the plasma between fast and slow streams and deflection of the SW velocity vector from westward (negative longitude angle φ) to eastward (positive φ) direction (e.g. see reviews by Gosling and Pizzo, 1999 and Tsurutani *et al.*, 2006, and references therein). The fast motion of interplanetary coronal mass ejections (ICMEs, including flux rope magnetic clouds (MCs) and non-MC ejecta) can interact with the surrounding SW and form a compression region before the ICME that is called the sheath.

We have recently calculated the average temporal profiles of several interplanetary and magnetospheric parameters for eight usual sequences of SW phenomena: (1) SW/CIR/SW, (2) SW/IS/CIR/SW, (3) SW/ejecta/SW, (4) SW/sheath/ejecta/SW, (5) SW/IS/sheath/ejecta/SW, (6) SW/MC/SW, (7) SW/sheath/MC/SW, and (8) SW/IS/sheath/MC/SW (where SW is the undisturbed solar wind, and IS means interplanetary shock) for the interval 1976–2000 (Yermolaev *et al.*, 2015). To calculate the average temporal profiles of the parameters in the phenomena with different durations, we use the method of double superposed epoch analysis: rescaling the time between points of the interval (proportionally increased or decreased) in such a way that the respective beginnings and ends for all intervals of a selected SW type coincide (Yermolaev *et al.*, 2010, 2015). Figure 1 summarizes the behavior of the longi-

tude, φ , and the latitude, ϑ , bulk velocity angles observed in eight different phenomenon sequences. Changes in longitude angle φ in CIRs (both CIR sub-types: with IS and without IS) agree with earlier observations (*e.g.* Gosling and Pizzo, 1999). In addition, we have for the first time analyzed the average temporal profiles of bulk velocity angles in sheaths and ICMEs and found that the angle φ in ICMEs changes from 2 to -2° , while in sheaths, it changes from -2 to 2° (similar to the change in CIRs), *i.e.* the streams in CIRs/sheaths and ICMEs deflect in the opposite directions (the angle φ shows large deflections in MCs and sheaths before them because of small statistics). This fact has been explained by the same mechanism as for CIRs: the interaction of a fast ICME with slow plasma in the SW before the sheath and the Sun's rotation. Two types of compression regions, CIRs and sheaths, are formed due to the velocity difference between the undisturbed SW and the leading edge of the corresponding piston (high-speed stream (HSS) or ICME), and they have identical average velocity profiles in value and in inclination; the speed profiles for cases with an IS are located $\approx 100 \text{ km s}^{-1}$ higher than for those without an IS, which indicates that the $\sim 100 \text{ km s}^{-1}$ increase in speed of the pistons leads to the formation of an IS (Yermolaev *et al.*, 2017).

When averaging the latitude angle, ϑ , on all intervals of a chosen SW type, we see that it is almost constant and $\sim 1^\circ$. We suggest that in contrast to the longitude angle, φ , which has one temporal profile for selected SW types, ϑ can have several different temporal profiles due to the various directions of motion of the pistons relative to the solar equator plane, and therefore the procedure of data processing we used did not allow us to select these profiles from total data set.

We select here for the first time intervals with four trends of the variation in ϑ (increasing, decreasing, positive, and negative) for various SW types and then calculate the average temporal profile for each trend. The organization of the article is as follows. Section 2 describes data and method. In Section 3 we present the results on the behavior of longitude φ and latitude ϑ bulk velocity angles in various SW types. Section 4 summarizes the results.

2. Data and Method

We used the same data and method as in our previous works (Yermolaev *et al.*, 2015, 2017): 1) the 1h interplanetary plasma and magnetic field data from the OMNI database (<http://omniweb.gsfc.nasa.gov>; King and Papitashvili, 2004), 2) our catalog of large-scale SW phenomena in the period 1976–2000 (<ftp://ftp.iki.rssi.ru/pub/omni/>; detailed information of the procedure to identify the phenomena is described in the article by Yermolaev *et al.*, 2009), and 3) the double superposed epoch analysis method (Yermolaev *et al.*, 2010). This method involves rescaling (proportionally increasing or decreasing the time between points) the duration of the interval for all SW types in such a manner that the respective beginnings and ends of all intervals of a selected type coincide. Similar methods of profile analysis were used by Yokoyama and Kamide (1997), Lepping *et al.* (2003), and Lepping, Berdichevsky, and Wu (2017).

We used the same set of SW events with small corrections: 1) we merged the data of two sets, MC and ejecta, and analyzed the total set of ICMEs as the statistics of MCs is small, and 2) we excluded several events that do not have angle measurements during all intervals. As a result, our analysis includes 355 events for CIRs, 350 for sheaths, and 357 for ICMEs.

We calculated the angles φ_1 and φ_2 , and ϑ_1 and ϑ_2 by averaging over the first and second half of each SW-type interval, respectively, and selected events with similar signs of the corresponding angles, *i.e.* $-/-$ (the angles in both halves of the interval are negative),

$-/+$ (the angle in the first half of the interval is negative and it is positive in the second half), $+/-$, and $+/+$. This approach allows us to estimate approximately the main deflection trend of a stream in each event and to select events with similar deflection. It should be noted that for the majority of data subsets, the statistics remains large enough for reliable results.

3. Results

In this section, we perform two types of analysis of the angles, φ and ϑ , in different types of SW. First, we study the trend of the angles, *i.e.* we investigate the relations of the longitude, φ_1 and φ_2 , and latitude, ϑ_1 and ϑ_2 , angles averaged, respectively, in the first and second halves of the intervals of the corresponding SW type. In this case, the time resolution of the averaged angles is 5–12 hours and allows us to only roughly estimate the trend. Then, based on the obtained trend, we select the events and study the detailed (with a time resolution of about 1 hour) behavior of the average angles for events with a corresponding trend.

3.1. Analysis of the φ and ϑ Trends

Figure 2 illustrates φ_1 and φ_2 for six SW types: (1) CIRs, (2) ISs/CIRs, (3) sheaths, (4) ISs/sheaths, (5) ICMs, and (6) ISs/ICMs. Numbers and percentages of events in four quadrants ($-/+$, $+/-$, $-/-$, and $+/+$) and in two half-planes ($\varphi_1 > \varphi_2$ and $\varphi_1 < \varphi_2$) for average φ_1 and φ_2 for the six different SW types are presented in Table 1. For CIRs, $\sim 4/5$ of the events have increasing φ ($\varphi_1 < \varphi_2$) and $\sim 1/2$ of the events are in the $-/+$ quadrant. These events result in the well-known average temporal profile of φ in CIRs (see top panels in Figure 1). Although there are fewer such events in sheaths than in CIRs ($\sim 2/3$ with $\varphi_1 < \varphi_2$ and $\sim 1/3$ in the $-/+$ quadrant, respectively), their relative number is enough to make the average profile of φ in sheaths look like the profile in CIRs. ICMs have approximately the same number of events as sheaths, but with the opposite trend, $\sim 2/3$ with $\varphi_1 > \varphi_2$ and $\sim 1/3$ in the $+/-$ quadrant. Therefore, the opposite trend of the average-angle profile is observed in ICMs.

In contrast to the longitude angle, φ , the latitude angle, ϑ , is fairly uniformly distributed over the quadrants and half-planes. Figure 3 presents the average ϑ_1 and ϑ_2 for the same six SW types: (1) CIRs, (2) ISs/CIRs, (3) sheaths, (4) ISs/sheaths, (5) ICMs, and (6) ISs/ICMs. The numbers and percentages of events in four quadrants and two half-planes are shown in Table 2. Most of the events for all SW types are located symmetrically near the line $\vartheta_1 = \vartheta_2$ and in the $+/+$ and $-/-$ quadrants (see Figure 3), *i.e.* $\sim 60\%$ of the events do not change the value and sign of ϑ for the corresponding SW type.

Figure 4 shows the deflection of the velocity vector in longitude and latitude planes (changes in angles $\Delta\vartheta = \vartheta_2 - \vartheta_1$ and $\Delta\varphi = \varphi_2 - \varphi_1$) in different SW types. The average values, standard deviations, and statistical errors in angle differences $\Delta\vartheta$ and $\Delta\varphi$ are presented in Table 3. The standard deviations for $\Delta\vartheta$ and $\Delta\varphi$ are similar and around 3° . Because the statistics are sufficiently high, the average values of the velocity vector deflection in the ecliptic plane exceed the statistical errors and indicate a systematic deflection in one direction for CIRs and sheaths and in the opposite direction for ICMs. In the meridional plane, the average angles of the velocity vector deflection are in general smaller than the statistical errors, and their distributions are symmetric relative to the radial direction.

Figure 5 shows the average direction of the velocity vector in the first (red) and second (blue) halves of the intervals for different SW types. Average values, standard deviations,

Figure 2 Distributions of average angles φ_2 and φ_1 for six different SW types as indicated in the upper right corners of the panels. For each panel we present the event percentages in the four quadrants.

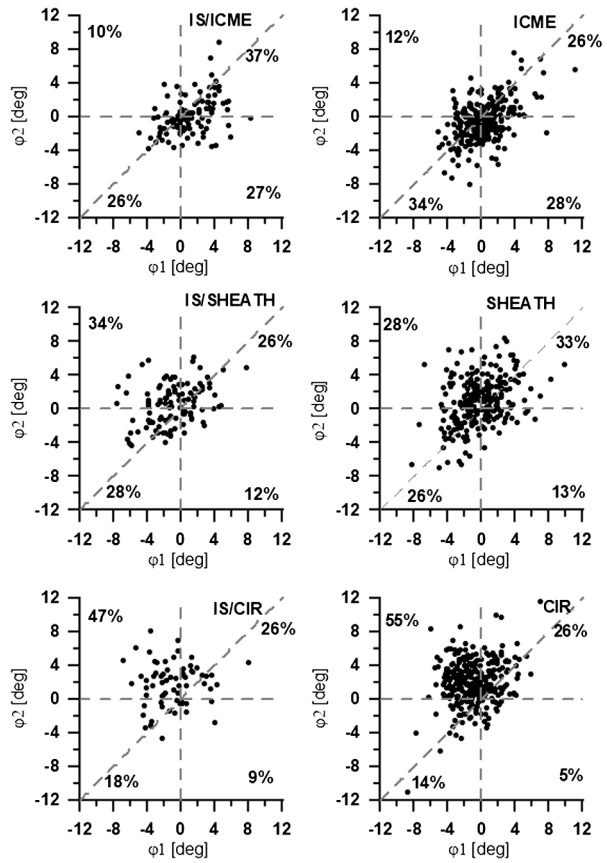


Table 1 Number and percentage of events in the four quadrants ($-/+$, $+/-$, $-/-$, and $+/+$) and in the two half-planes ($\varphi_1 > \varphi_2$ and $\varphi_1 < \varphi_2$) for average φ_1 and φ_2 for the six different SW types (see Figure 2).

SW type	Number of events (%)						
	All	$\varphi -/+$	$\varphi +/-$	$\varphi -/-$	$\varphi +/+$	$\varphi_1 > \varphi_2$	$\varphi_1 < \varphi_2$
CIR without IS	289	159 (55)	15 (5)	40 (14)	75 (26)	53 (18)	236 (82)
CIR with IS	66	31 (47)	6 (9)	12 (18)	17 (26)	16 (24)	50 (76)
Sheath without IS	243	69 (28)	31 (13)	62 (26)	81 (33)	85 (35)	158 (65)
Sheath with IS	107	36 (34)	13 (12)	30 (28)	28 (26)	38 (36)	69 (64)
ICME without IS	260	33 (12)	72 (28)	88 (34)	67 (26)	162 (62)	98 (38)
ICME with IS	100	10 (10)	27 (27)	26 (26)	37 (37)	64 (64)	36 (36)

and statistic errors of ϑ and φ in the first and second halves of the intervals for different SW types are presented in Table 4. The data in Figure 5 and Table 4 agree with the similar data in Figure 4 and Table 3, and in contrast with Figure 4 and Table 3, they give us additional information about the start and end values of the angles.

Figure 3 Distributions of average angles $\vartheta 2$ and $\vartheta 1$ for the six different SW types as indicated in the upper right corners of the panels. For each panel we present the event percentages in the four quadrants.

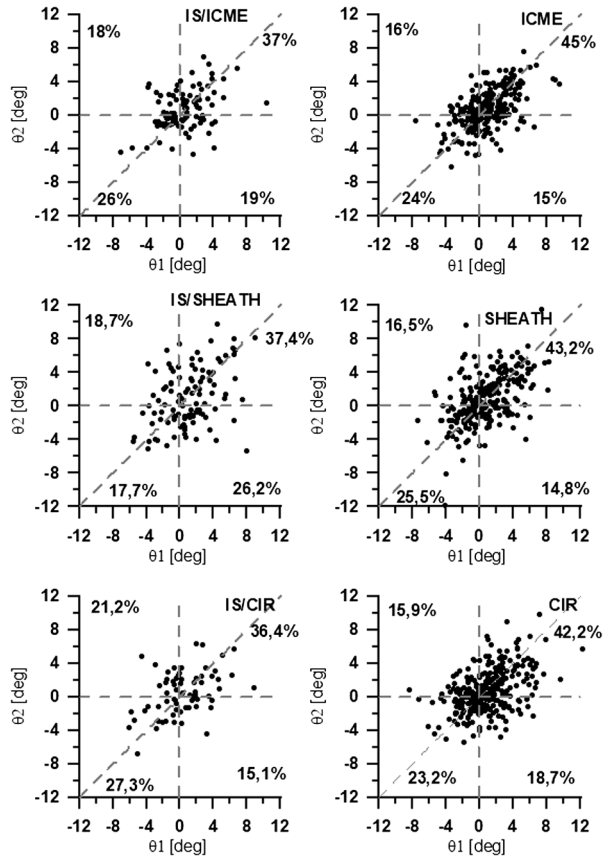


Table 2 Number and percentage of events in the four quadrants ($-/+$, $+/-$, $-/-$, and $+/+$) and in the two half-planes ($\vartheta 1 > \vartheta 2$ and $\vartheta 1 < \vartheta 2$) for average $\vartheta 1$ and $\vartheta 2$ for the six different SW types (see Figure 3).

SW type	Number of events (%)						
	All	$\vartheta -/+$	$\vartheta +/-$	$\vartheta -/-$	$\vartheta +/+$	$\vartheta 1 > \vartheta 2$	$\vartheta 1 < \vartheta 1$
CIR without IS	289	46 (16)	54 (19)	67 (23)	122 (42)	160 (55)	129 (45)
CIR with IS	66	14 (22)	10 (15)	18 (27)	24 (36)	34 (52)	32 (48)
Sheath without IS	243	40 (17)	36 (15)	62 (25)	105 (43)	108 (44)	135 (56)
Sheath with IS	107	20 (19)	28 (26)	19 (18)	40 (37)	52 (49)	55 (51)
ICME without IS	257	40 (16)	39 (15)	62 (24)	116 (45)	129 (50)	128 (50)
ICME with IS	100	18 (18)	19 (19)	26 (26)	37 (37)	41 (41)	59 (59)

3.2. Analysis of the Temporal Profiles of Angles φ and ϑ

In this subsection we analyze the average temporal profiles of φ and ϑ in different SW types when selecting the events with four different trends for ϑ : $-/+$, $+/-$, $-/-$, and $+/+$. It is to be noted that the event selection results in a significant decrease in the statistics

Figure 4 Difference distribution of average angles $\Delta\varphi = \varphi_2 - \varphi_1$ and $\Delta\vartheta = \vartheta_2 - \vartheta_1$ for the six different SW types.

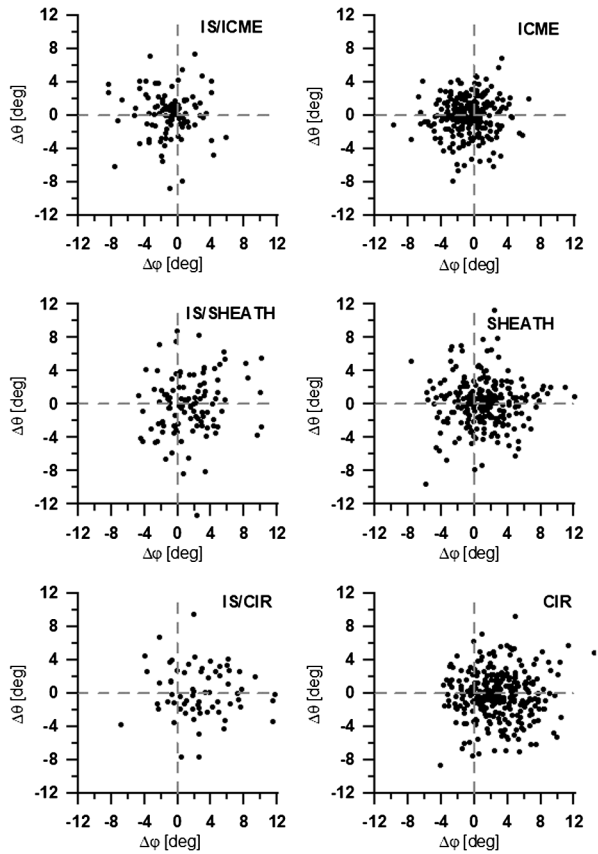


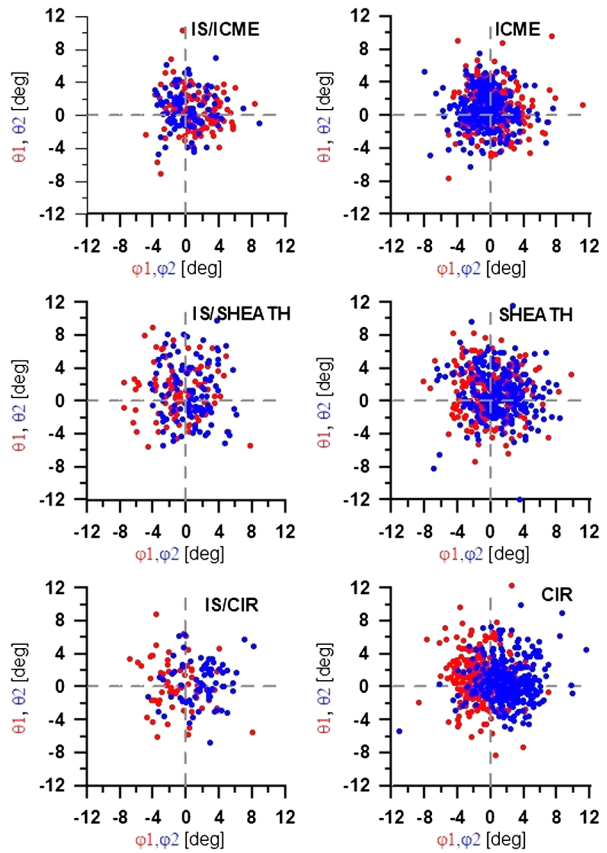
Table 3 Average values and standard deviations (statistic errors) for angular differences $\Delta\vartheta$ and $\Delta\phi$.

SW type	Number of events (N)	$\langle \Delta\vartheta \rangle \pm \sigma_{\Delta\vartheta} (\sigma_{\Delta\vartheta}/\sqrt{N})$	$\langle \Delta\phi \rangle \pm \sigma_{\Delta\phi} (\sigma_{\Delta\phi}/\sqrt{N})$
CIR without IS	289	$-0.26 \pm 2.83 (0.17)$	$2.90 \pm 3.17 (0.19)$
CIR with IS	66	$0.16 \pm 3.06 (0.38)$	$2.74 \pm 3.73 (0.46)$
Sheath without IS	243	$0.14 \pm 2.83 (0.18)$	$1.13 \pm 3.12 (0.30)$
Sheath with IS	107	$-0.05 \pm 3.62 (0.35)$	$1.43 \pm 3.14 (0.30)$
ICME without IS	257	$-0.12 \pm 2.56 (0.16)$	$-0.82 \pm 2.42 (0.15)$
ICME with IS	100	$0.17 \pm 2.77 (0.28)$	$-0.96 \pm 2.67 (0.27)$

and several profiles are not sufficiently smooth. Nevertheless, the obtained data allow us to conclude on the main features of the profiles.

Figure 6 shows the results obtained using the double superposed epoch analysis for CIRs. In all subsets, the angle φ has similar “integral-like” shapes and does not depend on the selection with ϑ . During increasing and decreasing trends of ϑ ($-/+$ and $+/-$), the average temporal profiles show changes but have similar shapes: first the absolute value of the angle increases, reaches a maximum, decreases to 0, and then has an analogous form with the

Figure 5 Stream directions in the first (red circles) and second (blue circles) halves of the intervals for different SW types.



opposite sign. For cases without trends (without a change in sign $+/+$ and $-/-$), the form for ϑ has a maximum or minimum in the middle of the interval, respectively.

Figure 7 shows the results obtained for the complex of events “sheaths + ICMEs”. The first and second columns of the figure present results when selecting the events in sheaths, and the third and fourth columns show events with the selection in ICMEs. The behavior of φ is similar to the one without selecting ϑ : in all subsets the angle φ has similar “integral-like” shape and does not depend on the selection of ϑ . The average temporal profiles of ϑ in sheaths and ICMEs behave the same way as in CIRs, in agreement with the trends $-/+$ or $+/-$. It is important to note that values of ϑ at the end of the sheath type correspond to the value at the beginning of ICME type: there are no discontinuities and events with increasing (decreasing) trend in sheaths have a similar shape as events with decreasing (increasing) trend in ICMEs (see, *e.g.* Figures 7b and 7k and Figures 7c and 7i).

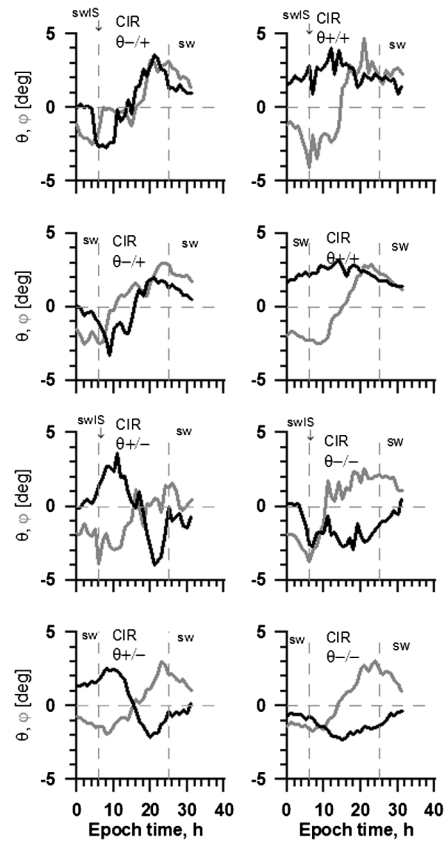
4. Discussion and Conclusions

We have statistically studied the variation in longitude and latitude velocity angles φ and ϑ in CIRs, sheaths, and ICMEs (both with and without interplanetary shocks before CIRs and sheaths) and obtained the following results:

Table 4 Average values and standard deviations (statistic errors) of angles ϑ and φ in the first and second halves of intervals for different SW types.

SW type	Number of events N	$\langle \vartheta 1 \rangle \pm \sigma_{\vartheta 1} (\sigma_{\vartheta 1} / \sqrt{N})$	$\langle \vartheta 2 \rangle \pm \sigma_{\vartheta 2} (\sigma_{\vartheta 2} / \sqrt{N})$	$\langle \varphi 1 \rangle \pm \sigma_{\varphi 1} (\sigma_{\varphi 1} / \sqrt{N})$	$\langle \varphi 2 \rangle \pm \sigma_{\varphi 2} (\sigma_{\varphi 2} / \sqrt{N})$
CIR without IS	289	0.94 ± 2.87 (0.17)	0.68 ± 2.52 (0.15)	-0.93 ± 2.49 (0.15)	1.94 ± 2.65 (0.16)
CIR with IS	66	0.35 ± 3.02 (0.37)	0.51 ± 2.66 (0.33)	-0.95 ± 2.78 (0.34)	1.79 ± 2.58 (0.32)
Sheath without IS	243	0.78 ± 2.82 (0.18)	0.92 ± 2.92 (0.19)	-0.24 ± 2.71 (0.17)	0.90 ± 2.81 (0.18)
Sheath with IS	107	1.17 ± 3.03 (0.29)	1.11 ± 3.46 (0.33)	-0.89 ± 2.90 (0.28)	0.54 ± 2.45 (0.24)
ICME without IS	257	0.84 ± 2.52 (0.16)	0.71 ± 2.31 (0.14)	0.28 ± 2.45 (0.15)	-0.51 ± 2.36 (0.15)
ICME with IS	100	0.46 ± 2.61 (0.26)	0.63 ± 2.32 (0.23)	1.10 ± 2.58 (0.26)	0.14 ± 2.28 (0.23)

Figure 6 Average temporal profiles of φ and ϑ for CIRs when selecting the events with trends of ϑ $-/+$, $-/-$, $+/+$, and $-/+$.



- i) For CIRs and sheaths, the numbers of events with an increasing trend in the longitude angle φ ($\varphi_1 < \varphi_2$) are about 80 and 65%, respectively, and the average time variation of the angle φ has an increasing “integral-like” form. The interaction of fast pistons (HSS or ICME) with the slow SW plasma before them and the solar rotation can explain this result. The difference in percentages can be connected with the non-radial motion of several ICMEs. For ICMEs, the number of events with a decreasing trend in φ is about 63%, and the average time variation of φ has a decreasing shape.
- ii) For all SW types, the number of events with increasing and decreasing trends in the latitude angle, ϑ , is small and approximately equal (about 15%), the number with a positive angle ($+/+$) is slightly higher than the number with a negative angle ($-/-$) (40% vs. 25%), therefore the average time variation of the angle ϑ is approximately constant and is about 1° .
- iii) The presence of interplanetary shocks before CIRs and sheaths has little effect on the above distribution of events.
- iv) For all cases of selection with ϑ , the average angle φ has the same shape in CIRs and sheaths, *i.e.* it does not depend on the selection with ϑ . In ICMEs the average profile of φ has an irregular shape (due to insufficiently high statistics) and tends to either decrease or be constant.
- v) For sheaths and CIRs with increasing and decreasing trends of ϑ (with a change in sign, $-/+$ and $+/-$), the form for ϑ is the same as for φ : first the absolute value of the

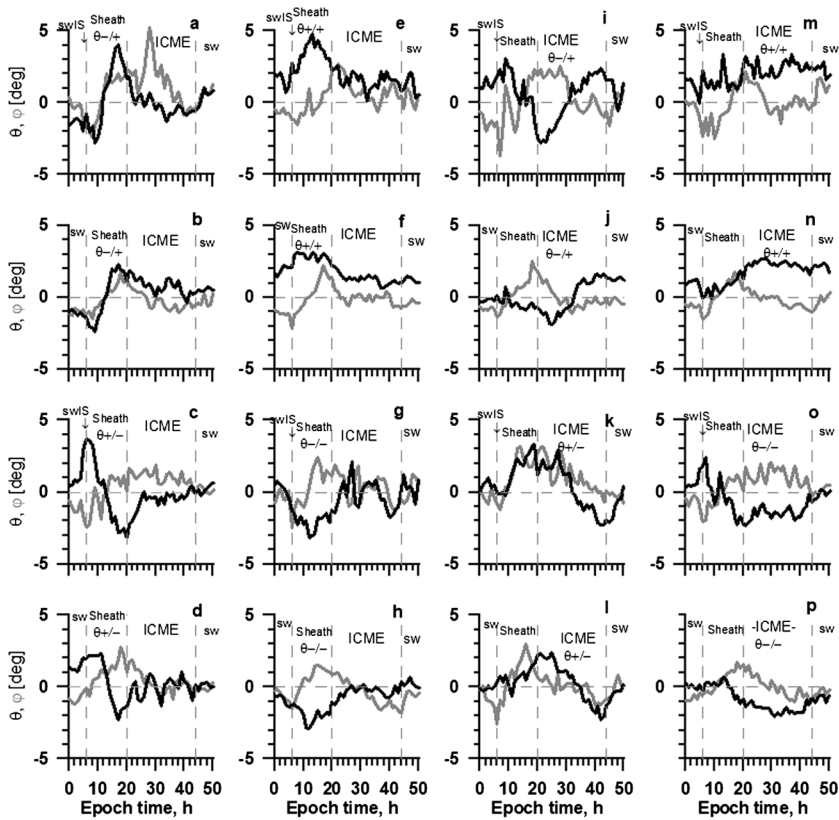


Figure 7 Average temporal profiles of φ and ϑ for sheaths and ICMEs when selecting the trend for ϑ $-/+$, $-/-$, $+/+$, and $-/+$ for sheaths (first and second columns) and ICMEs (third and fourth columns).

angle increases, reaches a maximum, decreases to 0, and then has a similar shape with the opposite sign. For cases without trends (without a change in sign, $+/+$ and $-/-$), the form of ϑ has a maximum or minimum in the middle of the interval.

- vi) For all cases of selection with ϑ in sheaths, the average values of ϑ in ICMEs are small and vary little in the interval. The values of ϑ at the end of the sheath and the beginning of the ICME are similar.
- vii) For all cases of selection with ϑ in ICMEs, the mean values of ϑ in sheaths are small and vary little in the interval. The values of ϑ at the end of the sheath and the beginning of ICME are similar.

The obtained results show that regardless of the type of piston, the interaction of large-scale SW streams leads to the same scenario of direction changes in the velocity vector in longitudinal and latitudinal planes, in agreement with the physical conditions in the interaction region. The observation of the deflection of the angles can be considered as a sign of these interactions.

Acknowledgements We thank the OMNI database team for the opportunity to use data obtained from the GSF/SPDF OMNIWeb (<http://omniweb.gsfc.nasa.gov>). YY is grateful to the SCOSTEP “Variability of the Sun and Its Terrestrial Impact” (VarSITI) program for support to participate in the first General Symposium

(VarSITI2016) in Albena, Bulgaria, 6–10 June, 2016. This work was supported by the Russian Science Foundation, project 16-12-10062.

Disclosure of Potential Conflicts of Interests The authors declare that they have no conflicts of interests.

References

- Gosling, J.T., Pizzo, V.J.: 1999, Formation and evolution of corotating interaction regions and their three dimensional structure. In: Balogh, A., Gosling, J.T., Jokipii, J.R., Kallenbach, R., Kunow, H. (eds.) *Corotating Interaction Regions. ISSI Space Scien. Ser. 7*, Springer, Dordrecht. DOI.
- King, J.H., Papitashvili, N.E.: 2004, Solar wind spatial scales in and comparisons of hourly wind and ACE plasma and magnetic field data. *J. Geophys. Res.* **110**(A2), A02209. DOI.
- Lepping, R.P., Berdichevsky, D.B., Szabo, A., Arqueros, C., Lazarus, A.J.: 2003, Profile of an average magnetic cloud at 1 AU for the quiet solar phase: WIND observations. *Solar Phys.* **212**, 425. DOI.
- Lepping, R.P., Berdichevsky, D.B., Wu, C.-C.: 2017, Average magnetic field magnitude profiles of wind magnetic clouds as a function of closest approach to the clouds' axes and comparison to model. *Solar Phys.* **292**, 27. DOI.
- Tsurutani, B.T., Gonzalez, W.D., Gonzalez, A.L.C., Guarnieri, F.L., Gopalswamy, N., Grande, M., Kamide, Y., Kasahara, Y., Lu, G., Mann, I., McPherron, R., Soraas, F., Vasyliunas, V.: 2006, Corotating solar wind streams and recurrent geomagnetic activity: A review. *J. Geophys. Res.* **111**, 0701. DOI.
- Yermolaev, Yu.I., Nikolaeva, N.S., Lodkina, I.G., Yermolaev, M.Yu.: 2009, Catalog of large-scale solar wind phenomena during 1976–2000. *Cosm. Res.* **47**(2), 81; Eng. transl. *Kosm. Issled.* **47**(2), 99. DOI.
- Yermolaev, Yu.I., Nikolaeva, N.S., Lodkina, I.G., Yermolaev, M.Yu.: 2010, Specific interplanetary conditions for CIR-, Sheath-, and ICME-induced geomagnetic storms obtained by double superposed epoch analysis. *Ann. Geophys.* **28**, 2177. DOI.
- Yermolaev, Y.I., Lodkina, I.G., Nikolaeva, N.S., Yermolaev, M.Y.: 2015, Dynamics of large-scale solar wind streams obtained by the double superposed epoch analysis. *J. Geophys. Res.* **120**(9), 7094. DOI.
- Yermolaev, Y.I., Lodkina, I.G., Nikolaeva, N.S., Yermolaev, M.Y.: 2017, Dynamics of large-scale solar-wind streams obtained by the double superposed epoch analysis: 2. Comparisons of CIRs vs. sheaths and MCs vs. ejecta. *Solar Phys.* **292**, 193. DOI.
- Yokoyama, N., Kamide, Y.: 1997, Statistical nature of geomagnetic storms. *J. Geophys. Res.* **102**(A7), 14215. DOI.